Available online at www.sciencedirect.com

SciVerse ScienceDirect

Physics Procedia 35 (2012) 162 – 167

Physics Procedia

Positron Studies of Defect 2011

2D-ACAR Studies on Swift Heavy Ion Si-Implanted GaAs

K. Sivaji[a,*], S. Selvakumar[a,b,c]

[a]*Materials Science Centre, Department of Nuclear Physics, University of Madras, Guindy Campus, Chennai 600 025, India.*
[b]*Center of Excellence in Antimatter Matter Studies, Research School of Physics and Engineering, Australian National University, Canberra 0200, Australia.*
[c]*Center of Excellence in Antimatter Matter Studies, Australian Nuclear Science and Technology Organisation Kirrawee 2232, Australia*

Abstract

Material properties modification by high energy heavy ion implantation is a prospective technology leading to many device fabrications. This technique induces defects and hence the physical properties of the materials are modified. The effects of swift heavy ion implantation induced defects by 120 MeV $^{28+}$Si ion implantation and doping in SI-GaAs are presented from the electron momentum distribution (EMD) of vacancy-type defects studied by two-dimensional angular correlation of annihilation radiation (2D-ACAR). The positron trapping due to the influence of high-energy Si- implantation in GaAs (*n*-type) is compared with the corresponding spectra of SI- GaAs and with Si-doped (*n*-type) GaAs. The EMD of the implanted sample shows a distinct increased isotropic distribution with a characteristic transform of its structure as evident from the low momentum region compared to the pristine sample. The characteristics of defects created by Si doping and by 120 MeV $^{28+}$Si ion implantation of undoped semi-insulating (SI) GaAS are discussed. These results indicate the nature of positron trapping in open volume defects such as vacancy clusters created by implantation.

Keywords: Positron Annihilation; 2D-ACAR, Heavy Ion Implantation, GaAs, Defects

1. Introduction

The effect of swift heavy ion (SHI) implantation in solids has been of increasing interest for a choice of various studies and applications for the last two decades, for both fundamental and applied aspects. MeV ion implantation in solids produces damages in the target material that leads to various effects. The effects are mainly material modifications, formation of surface craters and hillocks, amorphization, cracking, diffusion of dopants, void formation, crystallization, etc. Defects in crystals have a strong influence on the fundamental properties of semiconductors and play a significant role. Their presence can drastically modify the optical and electrical properties and influence the characteristics of electronic devices. As-grown GaAs consists of a multitude of native defects, vacancies in both the sub-lattices with deep level donors, etc, created during the crystal growth.

* Corresponding author. Tel.: +91 44 2220-2805; fax: +91 44 2235 0305.
E-mail address: sivaji@unom.ac.in, k_sivaji@yahoo.com.

1875-3892 doi:10.1016/j.phpro.2012.06.029

In the fabrication of semiconductor devices, one of the most widely used processes is low energy ion implantation for doping at the desired depth and concentration. Multilayered hetero-structure based devices and the requirement of deep implants necessitate MeV ion implantation [1] in view of the short range of heavy ions. Implantation of swift heavy ions into GaAs leads to the formation of defects consisting mainly of atoms displaced by a certain distance from their lattice sites. Although some reports exist in the literature on the low energy irradiation damage, no detailed studies have been carried out so far regarding the high-energy irradiation [2]. High-energy particles penetrate deep into the material and cause lattice damage in the form of vacancies, interstitials and defect complexes [3]. MeV irradiation of silicon into GaAs has been successfully employed to fabricate devices that require very wide or very deep *n*-type regions [4]. Silicon irradiation introduces simple point defects as well as more complex defects. MeV Si- implantation of GaAs at room temperature results in a very small amount of lattice disorder as a result of in-situ annealing leading to the formation of both perfect and partial interstitial types of dislocation loops [5].

Positron annihilation studies allow one to obtain finer details of the electronic structure of pure as well as defective solids than those possible by other conventional techniques [6-10]. Even though positron lifetime and Doppler broadening had been applied to defect characterization, the 2D-ACAR studies are expected to offer interesting results on the electronic structure of defects and a new perspective on defect characterization. 2D-ACAR constitutes a powerful technique of the electronic structure of the materials. Visualization of electronic structure of solids using positron annihilation allows one to understand the local electronic environment and to study defects at the atomic scale**.** Positron states at vacancies in (SI) GaAs and Si- doped GaAs samples were studied by Ambigapathy *et al* [11] for the charged vacancies and other point defects using 1.5 MeV electron irradiation at different sample temperatures [12]. Influence of defects on the electrical activation efficiency in Si- implanted (120 keV, 1×10^{14} cm^{-2}) and rapidly thermally-annealed GaAs was studied by Palmetshofer and Kastner [13]. The above studies indicate that Si- doping and low energy Si- implantation generate open volume defects associated with the Si- complexes.

In this paper, 2D-ACAR was used to map the electron momentum distribution (EMD) and to study the electronic structures of vacancies of high energy (120 MeV) Si- implanted (*n*-type) GaAs, Si- doped (*n*-type) GaAs and undoped (SI) GaAs samples. Since positrons are trapped by the open volume defects like vacancies and their complexes, their annihilation properties yield important information about the electronic structure of microstructural defects such as defect complexes, free volumes, etc. In the 2D-ACAR technique, a small angular deviation of the two 511 keV annihilation photons carries the information of the electron momentum at the time of annihilation of the electron-positron pair. This can be mapped two dimensionally using a pair of position sensitive detectors in coincidence, resulting in the two dimensional distribution $N(p_x,p_y)$ which is proportional to the projection of the two-photon momentum density $\rho^{2\gamma}(\mathbf{p})$. The resulting distribution of the electronic structure provides the symmetry. When defective materials are studied by positron techniques, a fraction of the positrons is trapped at vacancy defects in addition to the annihilation from delocalized bulk [6-10]. These trapped positrons at vacancies give the signature of defects through momentum distribution.

2. Experimental Details

The samples used for the present 2D-ACAR studies were undoped (SI) GaAs, Si-doped (*n*-type) GaAs and Si-implanted GaAs. The undoped (carrier concentration: 1 x 10^7 cm^{-3}) and Si- doped GaAs (carrier concentration: 1×10^{17} cm^{-3}) crystals were grown by the Liquid encapsulated Czochralski (LEC) method. The implanted sample was prepared by irradiating the above Si- doped GaAs with 120 MeV $^{28+}$Si- ions of fluence of $1x10^{13}$ cm^{-2} at RT from the 15 UD Pelletron tandem accelerator at the Inter University Accelerator Centre (formerly NSC) , New Delhi, India [14]. Crystals of 10×10 mm^2 size were used after polishing to mirror finish. These samples were mounted in a specially designed holder ≈ 3 mm away from the ^{22}Na positron source in a lead chamber such that the [100] direction was along the laboratory X- direction and [011] along the Y- direction. All the measurements were carried out at room temperature. The EMD measurements were carried out by the indigenously developed 2D-ACAR system based on position sensitive large area Anger cameras kept at 8 m apart from the sample under study [15]. The system is operational in coincidence for the 511 keV gamma events with a timing resolution of 30 ns. The system is facilitated with a CAMAC controlled multi-parameter data acquisition system, controlled by a personal computer monitored by an in-house data acquisition and analysis software for recording the positions (p_x,p_y) of the

annihilating gamma events. The acquired images are first stored in the computer memory as histograms as $N(p_x,p_y)$, after the focal plane transformations. Typically the data are obtained in steps of ~ 0.35 mrad (bin resolution) in the p_x and p_y directions projected to the p_z direction over an angular range of ± 22.5 mrad and displayed in the form of a histogram matrix of 128×128 bins. The bin resolution of the histogram is kept at ~80% of the angular resolution of 0.45 mrad. The resulting momentum distribution $N(p_x,p_y)$ of the positron-electron pair was integrated along the p_z direction corresponding to $[01\bar{1}]$.

3. Result and discussion

The EMD surface and contour plots of SI- GaAs compared to those of Si doped GaAs projected to $[01\bar{1}]$ are shown in Fig. 1(a) and Fig. 1(b), respectively, with p_x along [100] and p_y along [011] directions. The bone-like feature in low momentum region and the hexagonal feature in high momentum region are the characteristics of crystalline bulk semiconductors with a diamond structure [11]. The small central peak in the surface plot of SI-GaAs is due to the generation of native defects during the crystal growth process. The characteristic dips and valleys in the EMD of Bloch state e^- is clearly seen with a marked difference in the shape in the low momentum region between that for Si- doped and (SI) GaAs samples due to the positron trapping in open volume defects [11] and is rather isotropic upto ± 1.7 mrad (Fig.1b). However, the bone-like feature is less pronounced in the doped sample. In the higher momentum region, the hexagonal symmetry is retained. Despite these changes the part of the 2D-ACAR from Si- doped GaAs is bulk-like. These observations agree with the early 2D-ACAR results [12,16]. In the present study, these measurements on undoped and doped samples serve as a prelude to the measurements in Si-implanted GaAs sample.

A large number of vacancies are created due to high energy (120 MeV) Si- implantation in GaAs. The profile of vacancy concentration from the TRIM calculations and the projected range for 120 MeV Si- ions in GaAs corresponds to ~27 μm depth from the surface. Figure 2 shows SEM micrograph of the Si- implanted GaAs sample.

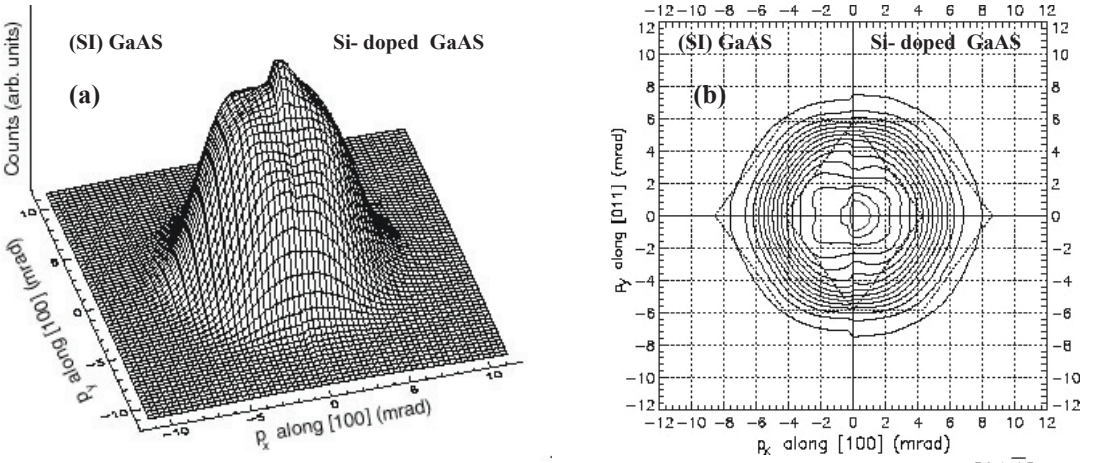

Fig. 1 Perspective (a) surface and (b) contour plots of 2D-ACAR spectrum $N(p_x,p_y)$ in a $[01\bar{1}]$ orientation for undoped (SI) GaAS (left half) and Si- doped (*n*-type) GaAS (right half).

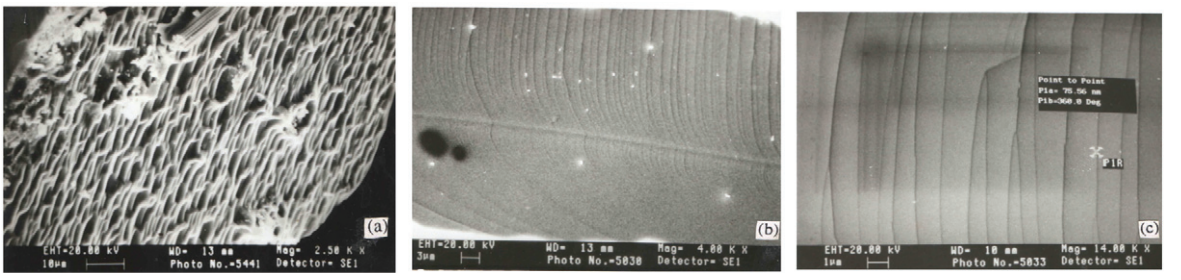

Fig. 2 SEM micrograph of 120 MeV silicon implanted AB etched GaAs - (a) Surface showing the implanted damage, (b) GaAs sample showing columnar structure at a magnification 4000, (c) magnification at 14,000.

Figure 2(a) shows the micrograph of surface, Fig. 2(b), 2(c) show the cross sectional views of two different magnifications. In Fig. 2(b), the top layer shows the end of range (EOR) of defects created by the implantation. Further it reveals that not only the EOR of the defects but also a few ions are extended from the EOR to the bottom due to high fluences. The implantation induced defects are analogous to columnar defects in the nanometer scale. These features are due to the coalescence of the implanted defects, which are parallel to the ion implanted direction and distributed throughout the damaged region. It consists of well-defined columnar structures of dimensions between 75 nm and 100 nm in diameter distributed throughout the entire implanted region as seen in Fig. 2(c).

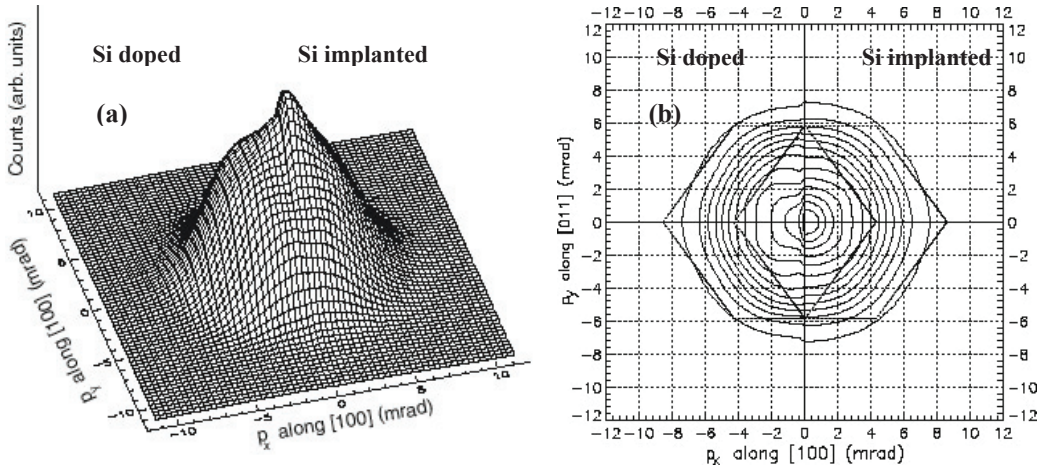

Fig. 3 Perspective surface and contour plots of 2D-ACAR spectrum N(p_x,p_y) in a $[01\bar{1}]$ orientation Si- doped (*n*-type) GaAS (left half) and Si- implanted (*n*-type) GaAS (right half) samples.

The surface and contour plots of 2D-ACAR measurements on Si- implanted GaAs sample are presented along with those of Si- doped sample in Figs. 3(a) and 3(b), respectively. Consequent to the implantation, the contribution in the low momentum region has considerably increased as seen in the surface plot of the EMD for Si- implanted GaAs. The corresponding contour plots (Fig. 3b) show a loss of the characteristic bone-like and hexagonal features and a circular distribution in the low momentum region has emerged indicating an isotropic EMD for the implanted sample due to the presence of a large number of defects. Furthermore the dips and valleys as present in the undoped and Si- doped GaAs samples (Fig. 1a) have disappeared.

The above mentioned differences among the EMDs of the three samples under study are brought out in the EMD cross-section for N(p_x,p_y= 0) as shown in Fig. 4. The width and amplitude of the distributions are listed in Table 1. In the total distribution, the amplitude increases with a decrease in width. On the other hand, the difference EMD extracted by subtracting the EMD of undoped GaAs from those of doped and implanted distributions, shows an increase in the width for the implanted case. An increase in the distribution in the low momentum region indicates positron trapping in open volume defects such as vacancy clusters due to 120 MeV Si- implantation. If this narrow momentum component increases in amplitude at the expense of its width, it can be attributed to the positronium formation in a sufficiently large open volume defect like a huge void. But in the present case, the width of the narrow component also increases along with the amplitude (Table 1). It suggests that the size of the positron trapping defects is not large enough to favour positronium formation but indicates an increase in the

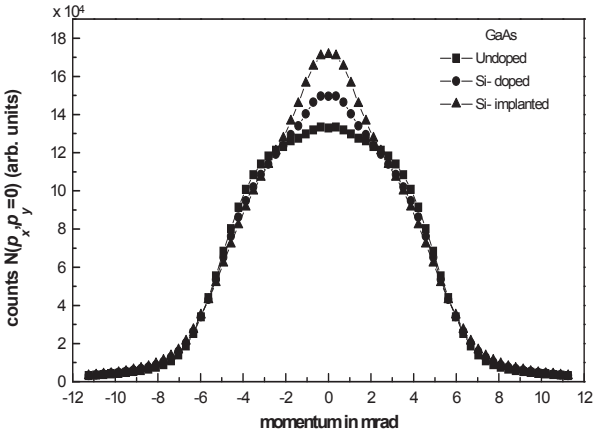

Fig. 4 Comparison of EMD cross sections of 2D-ACAR spectra for the undoped, Si- doped (*n*-type) and 120 MeV Si- implanted GaAs samples.

concentration of such positron traps. This is a clear evidence of the increase in the concentration of the open volume defects due to Si- doping [11] as well as implantation [3]. Lattice relaxation and lattice distortion occur around the defects [3,5,17] and the change of shape in the shoulder (i.e., valley) region can be attributed to such effects.

The line shape parameters, viz., *S*- and *W*- parameter of the EMD distribution curve can also be used to understand the quantitative information on positron trapping in defects as done earlier in the 2D-ACAR and Doppler broadening studies. The *S*- parameter corresponds to the valence annihilation and is defined as the relative number of annihilation events around the central region of the peak, while the *W*- parameter corresponds to the high momentum core electrons annihilation and is defined as relative number of annihilation events in the tail of the peak from the centroid. In 2D-ACAR experiments, ~ 4.0 mrad corresponds to 1 keV in the Doppler shift studies [4]. The *S*- parameter is calculated for the 4.92 mrad (1.23 keV) wide central region, the *W*- parameter at 5.27 mrad (1.32 keV) in the tail part of the 2D-ACAR distribution. The variation of normalized *S*- and *W*- parameters can be used to understand the presence of open volume defects. An increase (decrease) in the normalized *S*-(*W*-) parameter is believed to be due to an increase (decrease) in the concentration of open volume defects [11]. The calculated values of the parameters at 300 K are shown in Table 1. The normalized S parameter value of 1.10 for Si- implanted sample is more than the value of 1.05 for the Si- doped sample; the respective values of normalized *W* parameters are 0.92 and 0.97. These variations strongly support the above mentioned conclusion that the concentration of open volume associated defects should have increased remarkably due to high energy (~120 MeV) Si– implantation in Si doped GaAs and that the defect size would not be large enough to favour positronium formation.

Table 1 EMD parameters extracted from the N(p_x,p_y = 0) for various GaAs samples.

GaAs Sample	EMD along N(p_x,p_y= 0)			Difference EMD upto ±2.5 mrad			Calculated *S*- and *W*- Parameters		Normalised parameters	
	Area ×10^6	Width (mrad)	Amplitude	Area	Width (mrad)	Amplitude	*S*	*W*	$S_{dop(imp)}/S_{ref}$	$W_{dop(imp)}/W_{ref}$
Undoped (SI)	1.34	10.20	133400	-	-	-	0.4732	0.0329	1.00	1.00
Si- doped	1.36	9.49	149641	23675	2.4	16582	0.4952	0.0318	1.05	0.97
Si- implanted	1.41	8.09	171427	77507	2.8	38452	0.5214	0.0303	1.10	0.92

4. Conclusion

The heavy ion implantation introduces simple point defects as well as more complex defects. MeV Si-implantation results in a very small lattice relaxation and lattice distortion around the defects. It is apparent from the present 2D-ACAR studies on Si- doped and high energy Si- implanted GaAs samples that Si- incorporation either by doping or by ion implantation has induced significant open volume defects together with vacancy complexes and associated lattice distortions. The increased EMD peaks at the zero momentum region and the normalised S- and W-parameters extracted from the EMD clearly show that the concentration of such positron trapping defects has increased considerably due to high energy Si- implantation.

Acknowledgements

The authors acknowledge the financial support by the Department of Science and Technology and University Grants Commission, Govt. of India. S. Selvakumar acknowledges the CSIR-India for the award of Senior Research Fellowship (Award No. 9/115(666)/2007-EMR-I) and Australian Research Council (ARC) Centre of Excellence for supporting funds to present this work in international workshop on positron studies of defect-2011.

References

[1] D.C. Ingram, Nucl. Instr. and Meth. B 12, **161** (1985).
[2] F.D. Auret, A. Wilson, S.A. Goodman, G. Myberg and M.E. Meyer, Nucl. Instr. and Meth. B **90,** 387 (1994).
[3] Y.H. Aliyu, D.V. Morgan and R.W. Bunce, Phys. Stat. Sol. **135**, 119 (1993).
[4] C.M. Krowne and P.E. Thompson, Solid State Electron. **30**, 497 (1987).
[5] S. Chen, G. Braunstein and S.T. Lee, Proc. Mat. Res. Soc. Symp. **138**, 183 (1991).

[6] S. Berko, in: W. Brandt and A. Dupasquier (Eds.), *Positron Solid State Physics*, North-Holland, Amsterdam, p. 64, (1983).
[7] M. Eldrup, in: W. Brandt and A. Dupasquier (Eds.), *Positron Solid State Physics*, North-Holland, Amsterdam, p. 644, (1983).
[8] P.C. Jain, M. Eldrup, J.N. Sherwood, in: P.G. Coleman, S.C. Sharma, L.M. Diana (Eds.), *Positron Annihilation*, North Holland, Amsterdam, p. 674, (1982).
[9] M. Eldrup, N.J Pedersen, J.N. Sherwood, Phys. Rev. Lett. **43**, 1407, (1979).
[10] R. Krause-Rehberg, H.S. Leipner, '*Positron Annihilation in Semiconductors-Defect Studies*', Springer Series in Solid-State Sciences, (1998).
[11] R. Ambigapathy, A.A. Manuel, P. Hautojarvi, K. Saarieinen, and C. Corbel. Phys. Rev. B **50**, 2188 (1994).
[12] R. Ambigapathy, C. Corbel, P. Hautojarvi, A.A. Manuel, and K. Saarieinen, J. Phys. Cond. Matter **7**, L683 (1995).
[13] L. Palmeshofer and J. Kastner, Nuc. Instr. and Meth. B **59**, 1081 (1991).
[14] D. Kanjilal, S. Chopra, M.M. Narayanan, I.S. Iyer, V. Jha, R. Joshi and S.K. Datta, Nucl. Instr. and Meth. A **328,** 97 (1993).
[15] K. Sivaji, '*Two Dimensional Angular Correlation: System Development and Studies on Semiconductors*', Ph.D. Thesis, University of Madras (2000), unpublished.
[16] C. Corbel and F. Pierre, K. Saarinen and P. Hautojarvi, and P. Moser, Phy. Rev. B **45**, 3386 (1992).
[17] G. Braunstein, S. Chen, L.S. Tong, L.R. Zheng, K.Y. Ko, D.L. Peterson and D. Lawrence, Nucl. Instr. and Meth. B **59/60** 1032 (1991).